Critical speeding up of nonequilibrium electronic relaxation near nematic phase transition in unstrained Ba(Fe_{1−x}Co_{x})_{2}As_{2}

A. Patz, T. Li, L. Luo, X. Yang, S. Bud'ko, P. C. Canfield, I. E. Perakis, and J. Wang

Phys. Rev. B **95**, 165122 — Published 14 April 2017

DOI: 10.1103/PhysRevB.95.165122

Critical speeding-up of non-equilibrium electronic relaxation near Nematic phase transition in unstrained $Ba(Fe_{1-x}Co_x)_2As_2$

A. Patz,[1] T. Li,[1] L. Luo,[1] X. Yang,[1] S. Bud'ko,[1] P.C. Canfield,[1] I. E. Perakis,[2] and J. Wang[1]

[1]*Ames Laboratory - USDOE and Department of Physics and Astronomy, Iowa State University, Ames, Iowa 50011, USA*
[2]*Department of Physics, University of Alabama at Birmingham, Birmingham, Alabama 35294, U.S.A*

(Dated: March 20, 2017)

The origin of the anisotropic, paramagnetic phase associated with electronic nematicity in the iron pnictides is yet to be resolved. Furthermore, the detwinning technique used to study the nematic order in single crystals is known to introduce extra anisotropy into the sample, which can smear out the transition and even modify intrinsic characteristics associated with "spontaneous" Ising, Z_2, symmetry breaking. Here we use a strain and stress free, twinned sample to show that there is a significant reduction in the energy relaxation times of the hot electrons following non-equilibrium femtosecond laser excitation on both the high and low temperature sides of the nematic phase transition. This femtosecond, critical speeding-up behavior provides an alternative way to study complex, electronically-driven nematicity, invoking neither external strain nor measuring a small anisotropy in twinned crystals. Particularly, a detailed analysis of the observed ultrafast decay time and the amplitude associated with an initial electronic relaxation provides compelling implications on the physical origin of nematicity in iron pnictides: (1) nematic fluctuations strongly influence the dynamics of electron cooling; and (2) spin fluctuations determine the part of amplitude arising from the nematicity. Finally, we discuss ultrafast coherent phonon generation which may contribute to the measured transition temperature in our ultrafast measurements.

I. INTRODUCTION

Complex quantum materials often exhibit multiple distinct order parameters that are strongly intertwined in equilibrium, e.g., magnetic, superconducting, nematic, etc. Some recent prominent examples are seen in iron-arsenide based superconductors[1], which have reemphasized the importance of coupled and competing phases in determining the properties of complex materials. $Ba(Fe_{1-x}Co_x)_2As_2$ is a representative material in this class. It exhibits a multitude of interesting properties, including a structural phase transition (tetragonal–orthorhombic), spin–density–wave (SDW), superconductivity and electronic nematicity[2]. The nematic state of the iron pnictides gives rise to paramagnetic anisotropic regions in the phase diagram, above and even inside the superconducting dome. In particular, the high-temperature tetragonal symmetry (C_4) of the system is lowered to an orthorhombic one (C_2) at a temperature T_S driven by the divergence of electronic (nematic) fluctuations without lowing the magnetic symmetry (O_3)[3,4]. This electronically-driven nematic order has Ising (Z_2) character (two discrete values) which is theoretically predicted to have significant implications for the nature and type of the superconducting pairing mechanism and quantum criticality debated thus far[5]. Some of the open issues are how to detect critical divergence of the nematic fluctuations upon approaching the phase transition and how to disentangle the driving force of electronic nematicity between spin and orbit fluctuations. However, there are still formidable difficulties for answering these questions, especially when trying to do this by working close to quasi-equilibrium.

A major limitation of conventional equilibrium measurements, such as infrared spectroscopy[6] and electrical transport[7,8] has been that these experiments require an external force to break the C_4 symmetry in order to reveal the nematic state. This external force appears necessary because the presence of twin domains cancels out anisotropic signals in the bulk crystals probed by these methods. However, the de-twinning technique that breaks the tetragonal symmetry makes it difficult to reveal underlying intrinsic materials properties driven by spontaneously broken Ising symmetry. For example, measurements of de-twinned samples show a broad structural transition with orthorhombicity persisting up to even near room temperature in some cases. This likely contributes to some significantly contradictory results in the literature regarding the temperature of the nematic phase transition.

It is unclear at what temperature the nematic phase transition occurs, with some reporting very close to the structural transition[3,4] and other observing a transition far above it, e.g., ∼100 K as suggested in Ref.[9]. So far there are scarce quantitative methods to measure the nematic transition in strain/stress-free samples and more are needed to help answer this fundamental question.

Ultrafast optical spectroscopy represents a powerful tool for studying phase transitions in a complimentary fashion to conventional equilibrium probe methods[10–17]. Ultrafast spectroscopy can be used to potentially reveal temporal fluctuations of the nematic order parameter that would not be seen in static, time-averaged measurements. Prior femtosecond-resolved ellipsometry work measured residual in-plane anisotropy even in unstrained $Ba(Fe_{1-x}Co_x)_2As_2$ samples[4]. There, the dynamics displayed a characteristic two-step relaxation that allowed the separation of the anisotropy into its long-range magnetic order and nematic order components. Interestingly, a diverging recovery time for critical nematic fluctuations

was observed. However, quantitative analysis in the nematic phase was made difficult due to a limited signal-to-noise ratio, especially approaching to T_S. This prevented a precise determination of the temperature at which critical fluctuations appear.

In the present work, we demonstrate a different way to obtain key information about the electronic nematicity via femtosecond-resolved interband optical reflectivity $\Delta R/R$ in strain/stress free iron-pnictides. Different from the above mentioned anisotropic response, the present strategy is based on isotropic, hot electron energy relaxation and allows much larger signal-to-noise ratios. While this approach does not directly probe nematic order, its sensitivity to said order arises from the coupling between hot electrons and the spin-nematic degree of freedom. More specifically, it is found that heat is transferred from hot electrons to the spin-nematic reservoir with an electronic cooling time given by τ_{Fast} that is determined by the coupling. The fs electron cooling time is found to be strongly dependent on nematic fluctuations and nematic order. Therefore, by measuring the photoexcited electronic cooling, it becomes possible to gain more understanding of the electronic coupling with nematicity and to reveal signatures associated with nematic fluctuations in twin-domain crystals. One major advantage of this ultrafast differential reflectivity approach, is the increased signal-to-noise ratio.

In under–doped $Ba(Fe_{1-x}Co_x)_2As_2$[2], we observe a critical speeding-up of the relaxation time τ_{Fast} that is present on both the high and low temperature sides of the nematic phase transition. This speeding-up is absent in parent and optimally-doped compounds, likely because of the unique anisotropic, paramagnetic state in the under–doped sample. Moreover, a comparative analysis of the amplitude associated with the fs electron energy relaxation, defined as A_{Fast}, shows a non-monotonic temperature-dependence remarkably similar to low-frequency conductivity. The A_{Fast} amplitude shows an additional dependence on magnetic fluctuations peaked at T_N manifested as a crossover and downwards cusp going into the anisotropic nematic state. This crossover at T_N is only seen in the differential reflectivity ΔR/R however, and we believe this is because the low-frequency conductivity measurements we compare against are sensitive to only isotropic, average quantities and thus would not be sensitive to the nematic part of the signal. From the observed similarity and difference, we infer that interband optical nonlinearity originates from photo-induced spectral weight transfer due to Fermi surface (FS) renormalization, while the magnetic fluctuations determine the additional contribution to A_{Fast} near the nematic state.

This paper is organized as follows. In Section II, we present sample details and basic experimental characterizations. In Section III we show experimental results from fs-resolved interband optical reflectivity $\Delta R/R$ in strain/stress free iron-pnictide samples. In section IV, a detailed analysis of ultrafast signals is presented to underpin the effects from nematic and spin fluctuations. We also compare ultrafast dynamics in parent and optimally-doped samples. The final section concludes with a summary and broader outlook. Lastly, we provide raw data traces along with their fits to illustrate the high quality of fitting.

II. EXPERIMENTAL SCHEME

The samples used in this study were single-crystalline $Ba(Fe_{1-x}Co_x)_2As_2$ with cobalt substitutions of x = 0.00, 0.047 and 0.074 that represent undoped, under-doped and optimally doped samples, respectfully. The cobalt doped samples were grown out of an $(Fe_{1-y}Co_y)As$ flux using specifically deduced, high-temperature solution growth techniques[2,18]. To obtain the final cobalt concentration in the samples, elemental analysis was performed via wavelength dispersive x-ray spectroscopy (WDS) in the electron probe microanalyzer of a JEOL JXA-8200[18].

The underdoped x = 0.047 sample is our main focus for studying the electronic nematic state. Here, the high-temperature tetragonal C_4 symmetry of the system is lowered to orthorhombic C_2 at the temperature T_S = 66K before entering the spin-striped (0, π)/(π, 0) SDW transition at T_N = 48 K[19]. The anisotropic, paramagnetic state between T_S and T_N is characterized by a nematic order parameter that couples to various other degrees of freedom, such as magnetic fluctuations, lattice orthorhombicity, and orbital order[3]. Undoped and optimally doped samples do not exhibit the anisotropic paramagnetic state and are measured for comparison. In the undoped (x = 0.00) sample the paramagnetic-SDW transition temperature is almost indistinguishable from the tetragonal-orthorhombic transition temperature at $T_N \sim T_S \sim$ 136 K. The optimally doped (x = 0.074) sample on the other hand only exhibits a superconducting transition at T_C = 23 K.

Ultrafast differential reflectivity ΔR/R[20] data is taken using an ultrafast Ti:Sapphire laser amplifier producing 35 *fs* pulses (FWHM) with central wavelengths of 800 nm and repetition rate of 1 kHz. A beam splitter separated the laser output into pump and probe beams. The probe beam was frequency doubled to 3.1 eV with a BBO crystal and then focused onto the sample, while the pump beam was kept at the laser fundamental 1.55 eV. Spot sizes were chosen to be 670 μm and 330 μm for the pump and probe respectively. These spot sizes are much larger than the width of a single stripe-domain and therefore, the probe measures an average over both twin-domains. Unless otherwise noted, pump fluence was set to 115 μJcm^{-2} and probe wavelength was set to 400nm. Please note that such a pump fluence are chosen to have the perturbed, transient temperatures still close to the initial temperatures. A detailed explanation of the method used to extract the transient temperatures is based on the three-temperature model. We note that our calculation

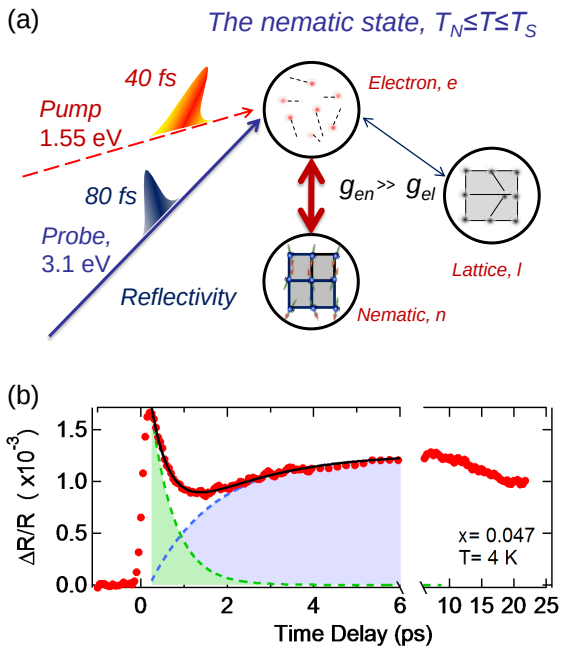

Figure 1: (a) Schematics of the experiment. Our ultrafast laser pump-probe experiment measures the photoexcited electron dynamics in iron-pnictides via a differential reflectivity ΔR/R technique. Differential reflectivity indirectly probes the nematicity by measuring the coupling between electron charge and nematic degrees of freedom characterized by g_{en} (b) A representative ΔR/R trace for measured $Ba(Fe_{1-x}Co_x)_2As_2$ samples (x = 0.047) is shown with a split x-axis. Photoexcitation causes a very fast change in reflectivity followed by an initial, fast fs decay (green fill) and a slow rising component (blue fill). Black line is the sum of fast decay and slow rising components. At longer timescales, ΔR/R shows a slow decay up to 300 ps. Pump=800nm, probe=400nm.

of the transient temperature includes coupling between electron, phonon, and spin heat baths which is important in our material because of strong electron-phonon and magneto-elastic coupling[4]. The incident pump and probe beams were linearly polarized and both beams were at near normal incidence with the sample. We detect pump-induced optical reflectivity change $\Delta R/R$ by probing the surface reflection $R = I_s + I_p$. We emphasize here that in twinned samples $\Delta R/R$ signals do not directly couple to the nematic order, but are indirectly coupled through hot electrons. Previous experiments show that pump-induced anisotropy changes, from subtracting the s and p polarized components $(I_s - I_p)$, are ~10 times smaller than optical reflection changes[4], i.e., $\Delta R/R \gg (\Delta R/R)_s - (\Delta R/R)_p$. However, the increased signal resolution on differential reflectivity measurements makes it possible to detect key signals originating from the coupling between hot electrons and the spin-nematic reservoir.

Fig. 1 illustrates our scheme for investigating hot electron energy relaxation to obtain key information on the electronic nematicity. This is achieved by exploiting photo-induced transient couplings between electronic and nematic reservoirs in the anisotropic, paramagnetic state of iron pnictides. Ultrafast pump excitation at 1.55 eV increases the transient temperature of the electronic heat bath with a time-dependence closely tracked by the rise of differential reflectivity, ΔR/R, during the first few ps. Subsequent to this rise, energy relaxation of hot electrons occurs as seen by the initial decay of the initial ΔR/R through heat transfer from the electron reservoir to nematic and phonon reservoirs. The rate of decay depends sensitively on the relative coupling strength between these coupled reservoirs. In conventional metals, such as copper, the electron energy relaxation is determined by the electron-phonon relaxation whereas in FeAs the electron energy relaxation is mostly dominated by the electronic-nematic coupling, which far exceeds the coupling of electron and phonon. Therefore, in FeAs, ultrafast photoexcitation results in a fast transfer of energy to the nematic reservoir that softens the nematic order[4]. In other words, the decrease in ΔR/R amplitude in the nematic state of FeAs directly relates to the transient electronic-nematic reservoir coupling and the corresponding relaxation time provides an unexplored way to probe nematic fluctuations unaffected by twinned domains.

III. EXPERIMENTAL RESULTS

A representative fs-resolved differential reflectivity trace ΔR/R for underdoped x = 0.047 sample is shown in Fig. 1(b). Note that the x-axis is split to illustrate both short and long time dynamics. Ultrafast photoexcitation heats up the electron reservoir, revealed by a rapid rise of ΔR/R, which is followed by two distinct processes: (i) an initial femtosecond relaxation of $\tau_{Fast} \sim 545$ fs and (ii) a slow rise of $\tau_{\rm slow} \sim 4.3$ ps. The final recovery of the ΔR/R will be presented in a later paper, but briefly occurs on much longer time scale as the system slowly recovers back to T = 4 K by heat diffusion within the laser pulse separation time of 1 ms. In order to analyze the short time relaxation components, we overlay the measured trace with a bi-exponential fitting function (black line) in Fig 1(b), given by:

$$f(t) = A_{Fast} \cdot e^{-t/\tau_{Fast}} + A_{Slow} \cdot (1 - e^{-t/\tau_{Slow}}) \quad (1)$$

where A_{Fast} and τ_{Fast} represent the respective amplitude and relaxation times of the fast component (green fill), and similarly for the slow components, A_{Slow} and τ_{Slow} (blue fill). This represents the minimum possible fitting parameters that give high-confidence fits for all sample dopings as discussed in Section IV.

Parameters extracted from fitting the underdoped sample demonstrate clear evidence of multiple phase transitions. First, critical fluctuations are observed in τ_{Fast} relaxation time as shown in Fig 2(c). The effects of temperature on τ_{Fast} can be separated into two

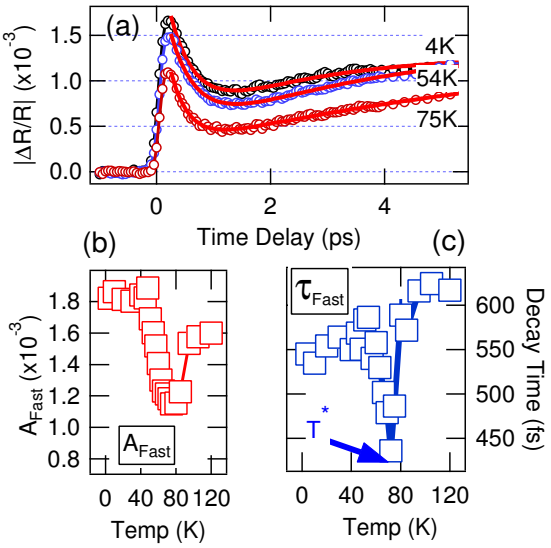

Figure 2: (a) Underdoped sample x = 0.047 temperature dependent Δ R/R data (black line, hollow circle) overlaid with bi-exponential fitting (red line) described in the text. Complete temperature dependence raw traces are shown in Fig. 12 in the Appendix. (b) Amplitude of the fast component amplitude A_{Fast} shows a complex, non-monotonic temperature dependence going across the phase transitions. (c) A critical speeding-up is seen in the τ_{Fast} relaxation time marking the Ising-Nematic transition temperature $T^* \sim 73.5$ K slightly above the tetragonal-orthorhombic transition temperature $T_N = 66$K.

components. One component is the non-critical background that slowly increases with temperature at a rate of $d\tau_{Fast}/d$T=0.56fs/K. The second component displays a sharp critical speeding-up with minimum 430fs occurring at $T^*\sim$73.5 K. This critical behavior is indicative of a second-order phase transition. The temperature range of critical fluctuations (ΔT=25K) is relatively narrow compared to temperature step-sizes used in previous ultrafast works reported, and could be one reason why this effect has not been reported on until now.

An unusual critical speeding-up behavior has been observed in prior works, including spin-ice compounds near their monopole liquid-gas transitions and ultrafast flourescence lifetime across the α-β transition of resorcinol.[21,22] In the present study, as the nematic temperature is approached, additional electronic relaxation pathways become available to the hot electrons that are photoexcited with 1.55eV pump photons. The addition of available relaxation channels to these hot electrons appears to most significantly influence the fast relaxation process as reflected in the obviously sharp critical speeding-up in τ_{Fast}. It is likely that large nematic fluctuations that sets in approaching to the nematic transition are responsible for it due in part to the coupling between the hot electrons to the nematic degree of freedom. Outside of the critical region, nematic fluctuations die out and as a result τ_{Fast} increases back up again.

The critical speeding-up of τ_{Fast} may also be quantitatively represented through phenomenological dynamical scaling as $\tau_{Fast} = |T/T^* - 1|^{-\nu z}$, where v and z are critical exponents representing correlation length and dynamical exponent, respectively. The best fit (see Fig. 11 in Appendix) gives values of vz = -0.1395 and T*=73.5. Importantly, this temperature is above magnetic phase transition at T_N=48K and structural phase transition at T_S=66K, which were carefully characterized via resistivity measurements on the same sample. Our data indicates the observed τ_{Fast} criticality at T^* corresponds to the nematic transition temperature because of its close proximity to T_S, which was theoretically predicted.[3] Further evidence linking the fast component to nematicity is evident from the temperature dependence of A_{Fast} discussed next.

Fig 2(b) shows A_{Fast} as function of temperature. A_{Fast} is nearly constant from 4K to the magnetic transition temperature, $T_N = 48$K. It is noteworthy that negligible changes are observed crossing the superconducting temperature as expected for the moderately high pump fluences of 115 μJcm^{-2} used here[11]. As temperature increases to the anisotropic paramagnetic state above T_N, a clear crossover is observed in which the amplitude begins to gradually decrease with temperature. The decrease of A_{Fast} continues until just above T_S, where the amplitude flattens out and then increases as temperature goes up to ~100 K. From there on, A_{Fast} remains nearly constant with temperature.

Surprisingly, the complex temperature dependence of A_{Fast} is also observed in low frequency conductivity measurements such as the Drude scattering rate Γ_N (blue square, Fig 3(b)) extracted from far-infrared conductivity[24,25]. The establishment of the nematic order parameter has been shown to result in an unusually broadband spectral weight redistribution from the far-infrared intra-band to the inter-band, optical regions[6]. This redistribution of spectral weight likely explains the unusual correlation between low energy FS reconstruction and high-energy ultrafast optical measurements for temperatures near the nematic phase transition. The ultrafast photoexcitation softens the nematic order, changing its fluctuations and giving rise to a photoinduced spectral weight transfer between FS states and high-energy optical states. In addition to results here showing the ultrafast optical nonlinearity at ~3.1 eV is sensitive to FS renormalization, it is well known from previous ultrafast studies on iron-pnictides that the ultrafast pump-probe technique can measure FS signatures even with such high-energy probes.[4,15,32?]

In the present study we find, in addition to the apparent similarity, an intriguing difference in the anisotropic paramagnetic state where nematicity sets in. The amplitude A_{Fast} remains constant up to T_N where a crossover and downward cusp going into the anisotropic paramagnetic phase occurs. This is not seen in the isotropic

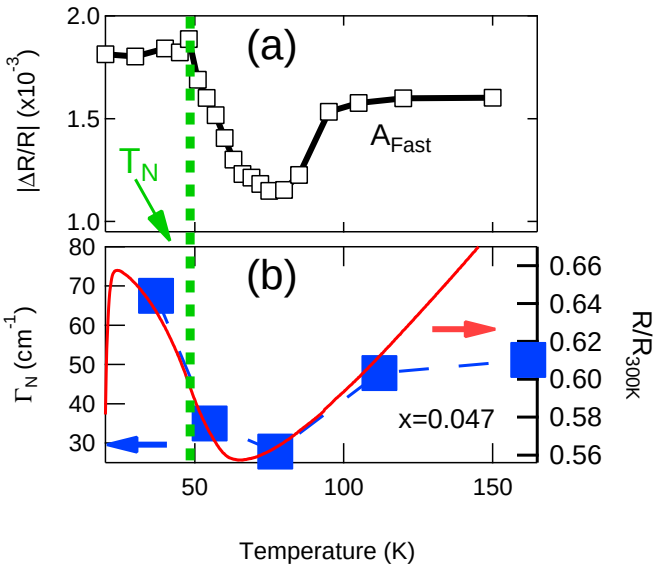

Figure 3: (a) Temperature dependence of the amplitude A_{Fast} (black square) extracted from the bi-exponential fitting of the underdoped sample, x = 0.047. (b) Scattering rate of narrow-Drude component (blue square) extracted in FTIR measurements by Lucarelli *et., al.* and DC-resistivity (red line) show a strikingly similar trend, which is a U-shaped feature bottoming out near T_S, and then flat until $\sim 150K$[24,25]. Green dashed line signifies T_N where A_{Fast} exhibits a clear crossover that is not seen in the traces shown in (b).

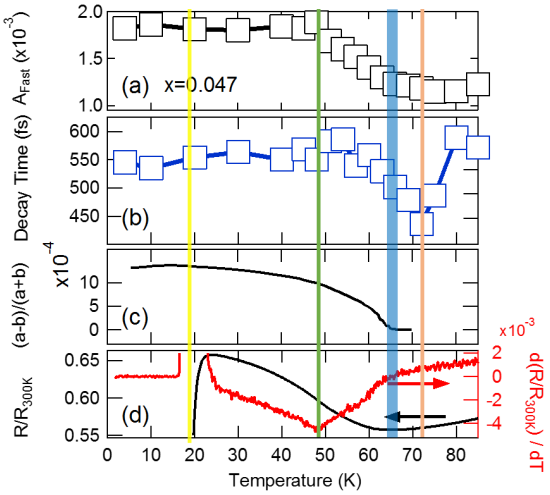

Figure 4: Key measurements indicating phase transition temperatures in underdoped sample (a) Temperature dependence of the amplitude A_{Fast} extracted from the bi-exponential fitting of the underdoped sample, x = 0.047. (b) A critical speeding-up is seen in the τ_{fast} relaxation time marking the experimentally extracted, critical temperature $T^* = 73.5$ K. (c) Anisotropic lattice parameters measured with X-ray diffraction show a structural transition occurring at $T_S \sim 66$ K.[19] (d) Resistivity normalized to its value at 300 K (black line) on the left axis and its derivative (red line) on the right axis show $T_C = 17$ K, $T_N = 48$ K and $T_S \sim 66$ K. The vertical yellow line marks T_C, green line T_N, blue line T_S and orange line T^*.

low-energy measurements Γ_N or ρ_{DC}. We believe the difference is caused by nematicity, which is sensed in the $\Delta R/R$ measurement but absent in resistivity and Drude-component. The difference between A_{Fast} and resistivity/Drude-component is most pronounced at T_N, and we infer that this is because magnetic fluctuations from the nematic contribution are also peaked at T_N. This provides further evidence in support of a magnetic fluctuation driven nematic scenario for the anisotropic iron-pnictides[27,28]. The good T_N agreement here is also a good indication that pump fluences used in this study were sufficiently low to not impart significant local lattice heating.

Importantly, the fast component amplitude contains magnetic signatures clear from the peak at $T_N = 48$K and the fast component also exhibits a critical speeding-up feature at $T^* \sim T_S$. This strong connection to magnetism and lattice degrees of freedom provides strong evidence that the fast component is strongly associated with nematicity.

Note that different behavior between $\Delta R/R$ and DC optical conductivity would not be unusual because of the different transitions probed. The connection between the measurements as shown here underscores the importance of the remarkable correlations in the nematic state of $Ba(Fe_{1-x}Co_x)_2As_2$. The above result corroborates our interpretation of the nematic order as its origin. A quantitative, microscopic connection between DC-conductivity and high energy pump-probe measurement is beyond the scope of this paper, but our work motivates further studies towards a deeper understanding of correlated materials driven out of equilibrium. Here we let the data speak for itself and point out the striking similarity and call attention to the difference which is peaked at T_N. One should note that the main features can be seen in the raw data in Figs. 2 and 3, that show the salient features directly in the temperature dependent cooling times and amplitudes. In addition, please note that there is an sharp upturn in ρ_{DC} above ~120K that are absent in both A_{Fast} and Γ_N with a flat temperature dependence. This can be attribute to that more trivial reasons that Γ_N is mostly responsible for shaping the temperature dependence of the coherent portion of DC-resistivity, while many other intrinsic and extrinsic factors can contribute to ρ_{DC} as incoherent portions, e.g., from phonons and disorders. Therefore, we have restricted our analysis to temperatures where total measured resistivity does actually follow the same trend as Γ_N, as seen in the Figure 3(b). Thus, in this temperature range the coherent portion of resistivity dominates the temperature dependence of total resistivity which make the analysis of the difference among A_{Fast}, ρ_{DC} and Γ_N more valid.

Now we take a closer look at the temperature dependence of τ_{Fast} to underpin the measured transition temperature T*, arising from dynamic critical nematic fluctuations, related to the structural phase transition. Seen in Fig 4 are the temperature dependence of (a) A_{Fast} amplitude, (b) τ_{Fast} decay time, (c) X-ray orthorhombicity from Nandi et al.,[19] and (d) DC-resistivity ρ (black line, left axis) along with its derivative $d\rho/dt$ (red line, right axis) shown up to temperatures of 85 K. It is clear from resistivity data that the superconducting transition temperature is 17 K (yellow bar) and SDW transition temperature is 48 K (green bar). X-ray diffraction and resistivity show that the orthorhombic-tetragonal structural phase transition occurs at ∼66 K (light blue bar). These transition temperatures are also consistent with other reported values for the 4.7% Co-doped compound[29]. Our results show that the critical speeding-up of hot electron relaxation τ_{Fast} appears just above the structural transition temperature by 6K. The good T_N agreement in Fig. 4(a) excludes any heating as the origin.

We argue that the measured transition temperature T* intimately correlates with the structural phase transition temperature T_S, i.e., they are driven by the same divergence of electronic fluctuations as discussed by Fernandes et. al[3]. The small discrepancy between the values in our ultrafast and static measurements is likely due to the effects from pump excitation, and most likely is due to ultrafast coherent phonon generation. Ultrafast photoexcitations create non-equilibrium carrier occupations, which are subsequently thermalized into hot electrons which generate phonons through the carrier-phonon interaction, i.e., displacive excitation of coherent phonons (DECP) mechanism[31]. Prior ultrafast spectroscopy measurements in $BaFe_2As_2$ provide evidence of a rapid increase in transition temperatures of macroscopic orders T_S/T_N on small ion displacement[17]. This is expected from the large magnetoelastic coupling in pnictides[4]. In the current sample, we also observe pronounced pump-induced phonon oscillations that likely act to transiently stabilize the ordered phase up to $\sim 6K$ above the static transition temperatures. These coherent phonons oscillation amplitudes exhibit a complex fluence and probe wavelength dependence as shown in the discussion section.

The intrinsic nematic phase transition has proven very difficult to precisely determine and most techniques use a mechanical strain/stress to detwin the sample. Previous measurements on detwinned samples have mostly shown that a nematic phase transition occurs far above the structural transition, e.g., at ∼250 K in optical measurements[30] and transport[7,8]. In addition, there are also some claims, still controversial, that the nematicity develops well above T_S by ∼100 K[9]. Our high-sensitivity, ultrafast spectroscopy measurement of a critical speeding-up clearly shows that the spontaneous nematicity sets in very close to the structural transition temperature in the strain/stress free samples.

IV. DISCUSSIONS

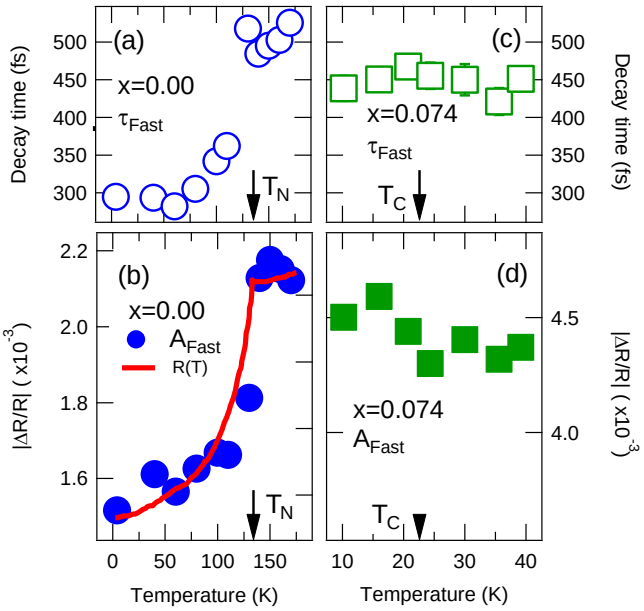

Figure 5: (a) Temperature dependence of the undoped x = 0.00 sample decay time τ_{Fast} and the (b) amplitude A_{Fast} (blue circle) overlaid with DC-resistivity (red line) and narrow-Drude component (need to add). All features are mostly constant from 4-110 K, whereafter a gradual is seen with increasing temperature up to the joint magneto-structural transition temperature. (c,d) Optimal doped sample with x = 0.074 showing extracted fast decay τ_{Fast} and corresponding fast amplitude A_{Fast}. No dependence on temperature is observed.

Next, for comparison we present differential reflectivity measurements on the undoped (x = 0.00) and the optimally doped (x = 0.074) samples. The raw traces and bi-exponential fitting can be found in the Appendix section. We note that our results from all samples can be fit similarly well with the bi-exponential fitting function described Section III. Figs. 5(a)-(d) summarize the detailed temperature dependence of the extracted decay time τ_{Fast} and amplitude A_{Fast} for both undoped and optimally doped compounds. The contrast with the behavior observed in the underdoped sample is clear. The control samples shown in Fig. 5 don't exhibit any anisotropic paramagnetic phase in thermodynamic measurements, which leads to our observation of distinctly different behaviors and the absence of the critical speeding-up seen in the underdoped compound. Concentrating on the undoped compound first, τ_{Fast} and A_{Fast} in this sample remain mostly constant from 4–100 K, and then gradually increases, with a broad crossover near the joint magneto-structural phase transition temperatures T_N, T_S ≈136 K. All these behaviors are opposite

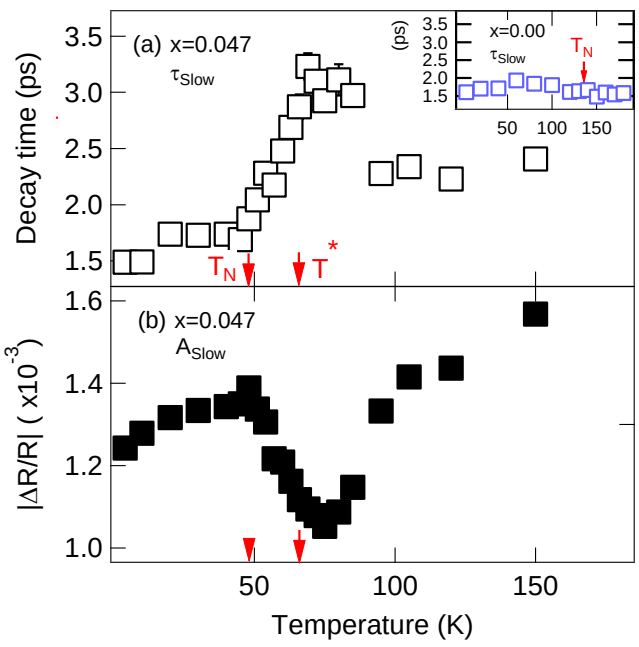

Figure 6: Slow, picosecond components of the underdoped sample. It is clear that the phase transitions affect not only the fast components but also the slow components (a) τ_{Slow} and (b) A_{Slow}. The inset of (a) shows τ_{Slow} component for the undoped sample, which exhibits no temperature dependence across the magneto-structural phase transition.

to those of the underdoped compound, which exhibit a reduction of both τ_{fast} and A_{fast} as the sample enters the anisotropic, paramagnetic state at T_N. Note that the upturn trend observed in the undoped compound is manifested as a slow-down approaching the magneto-structural transition, and is again similar to behaviors observed in DC-resistivity ρ_{dc} and low frequency conductivity. The above observations allows us to attribute the optical nonlinearity here to pump-induced softening of the mid-infrared SDW gap that gives rise to broadband photo-induced spectral weight redistribution of the FS and interband optical range. For further comparison, τ_{Fast} and A_{Fast} for the optimal doped compound is shown in Figs. 5(c) and 5(d). No change of the signals is observed for all temperatures measured in the optimally doped compound, indicating that the ultrafast differential probe at the current condition of moderately high pumping is not sensitive to the superconducting phase transition, but mostly to changes related to the SDW or orthorhombic phase transition. These results clearly show that the critical speeding-up is exclusively associated with the anisotropic, paramagnetic phase in the underdoped sample.

Next we briefly discuss the slow, picosecond relaxation components, A_{Slow} and τ_{Slow} observed in the differential reflectivity profile of underdoped compounds. Unlike the fs $\Delta R/R$ signals that exclusively follow the transient temperature T_e of the electronic heat bath, as established in many prior ultrafast studies in iron-arsenides and elemental metals, the slow, ps $\Delta R/R$ signals are influenced by many other extrinsic and intrinsic factors, ranging from defect states to heat diffusion and band structure changes. Nevertheless, in the underdoped sample here τ_{Slow} shows a maximum approaching the nematic phase transition. This is compared with τ_{Slow} for the undoped sample which shows negligible temperature dependence (inset). The temperature dependence of the amplitude A_{Slow} follows a similar trend as A_{Fast} which indicates this ultrafast optical nonlinearity component is influenced strongly by similar nematic signals as well. Further investigation is required to understand the complex interplay of extrinsic and intrinsic factors that effect the slow components, which is not the main focus of our current paper.

Finally, we briefly comment on the fitting models used. We note that the second component in Eqn. (1) can be interpreted physically as either a delayed rise or as a negative amplitude exponential decay with a constant positive offset (i.e. $-A_{Slow}\cdot e^{-t/\tau_{Slow}} + A_{Slow}$). Both physical interpretations are mathematically equivalent. Previous works have followed the latter interpretation and have not constrained the offset amplitude to necessarily be equal to the amplitude of the negative exponential (i.e. $-C\cdot e^{-t/\tau} + D$, with C≠D). This is necessary to fit traces where the $\Delta R/R$ signal becomes negative[32]. Here, we don't observe this negative $\Delta R/R$ in any doping of our samples, and therefore we choose to constrain the amplitudes of the offset and negative exponential to be equal.

Fig 7(a) illustrates typical coherent oscillations observed at short timescales in the pump-probe reflectivity measurements. The probe wavelength here was set to 975nm and temperature 4K although the oscillation was observed for all wavelengths, temperatures, and samples measured. The calculated FFT spectrum of the residual bi-exponential fitting from Fig 7(b) is shown in inset and shows clear oscillation peak at 5.5THz corresponding to the A_{1G} mode. The amplitude of the A_{1G} oscillation amplitude scales linearly with $\Delta R/R$ amplitude, and both amplitudes scale linearly with power as shown in Fig 7(b).

To study the wavelength dependence a 3mm thick sapphire crystal is inserted into a new path of the laser 800nm output, which generates a white-light continuum probe from 400nm to 1300nm. The complex probe wavelength dependence is shown in Fig 8(a), showing a pronounced increase in phonon amplitude for wavelengths longer than the 800nm pump. Interestingly, the amplitude of $\Delta R/R$ shows the opposite trend, which is a pronounced decrease in amplitude above 800nm. This suggests that the higher energy probe is more sensitive to electronic dynamics while the low energy probe is more sensitive to the phonon dynamics. Likely, high energy photons are less coupled to FS electrons and thus less coupled to A_{1G} phonons which are believed to be strongly coupled to the FS.[4,33]

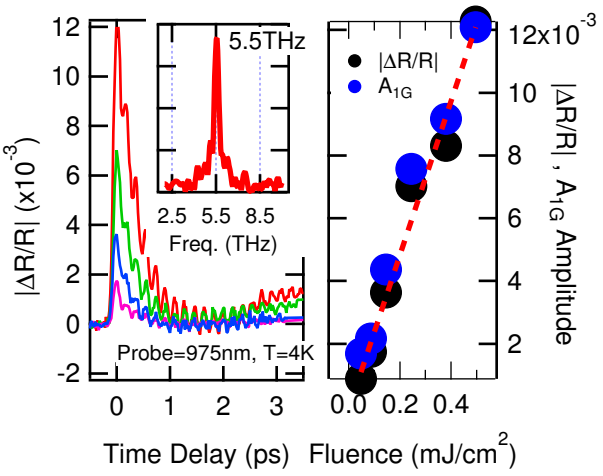

Figure 7: Fluence dependence of $\Delta R/R$ and the photoexcited 5.5THz A_{1G} phonon at 4K (a) Representative traces as function of fluence for 1.7mW(red), 840uW (green), 500uW(blue), and 300uW(magenta). Traces show the strong phonon oscillation and illustrates the phase does not shift for all pump fluences. Inset: FFT spectrum of the residual from the bi-exponential fitting shows strong peak at 5.5THz. This example was for 1.3mW pump power. (b) Both $\Delta R/R$ and the A_{1G} phonon amplitudes scale linearly with pump fluence. Here data is taken at 4K, on optimal doped sample, and probe=975nm.

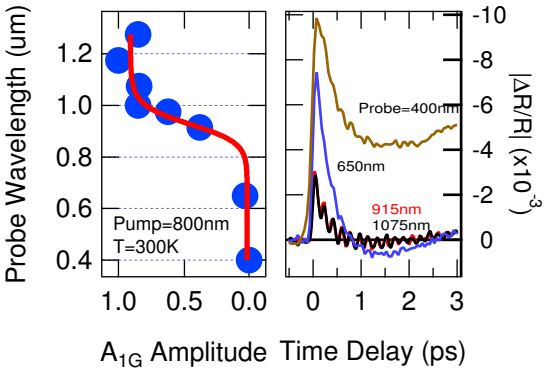

Figure 8: Wavelength dependence of photoexcited 5.5THz A_{1G} phonon (a) Amplitude of the 5.5THz oscillation as function of wavelength from 400nm to 1275nm. Red line is guide for the eye. (b) Some raw traces illustrating the trends seen.

V. CONCLUSIONS AND OUTLOOK

We discover a femtosecond critical speeding-up behavior of hot electron energy relaxation by using ultrafast optical spectroscopy. We show that this represents a powerful tool to study and understand the complex, electronically-driven nematic phase transition, without invoking external strain nor measuring small anisotropy in twinned crystals. The temporal dynamics of the nematicity, hidden in static measurements, shine new light on several outstanding issues associated such as the transition temperature and the origin. These results demonstrate, particularly, that nematic fluctuations strongly influence the electron cooling times and spin fluctuations determine the part of the relaxation component associated with the nematicity.

This work was supported by the Army Research Office under award W911NF-15-1-0135 (ultrafast non-equilibrium study). The initial, exploratory work was supported by W911NF-14-1-0656 (STIR program). The authors are greatly benefitted by the discussions in the workshop funded by W911NF-15-1-0016. Materials synthesis and basic sample characterization were supported in part by the Ames Laboratory, the US Department of Energy, Office of Science, Basic Energy Sciences, Materials Science and Engineering Division. Ames Laboratory is operated for the US DOE by Iowa State University under contract #DE-AC02-07CH11358. We thank Rafael Fernandes and Joerg Schmalian for for helpful discussions.

APPENDIX

We present raw differential reflectivity traces for the undoped sample from T = 4 K up to 150 K in Figure 7. We fit traces with the bi-exponential function over the range from time-zero to ∼12 ps. At 12 ps there is a local maximum, whereafter the signal decays up to long times, measured up to 300 ps in this work.

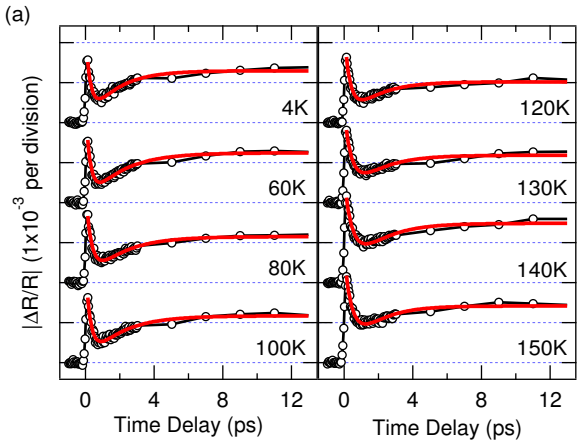

Figure 9: Temperature dependent differential reflectivity traces for the undoped sample (black line, black circle) overlaid with the bi-exponential fit function (red line) described in the main text.

Raw data for the optimally doped sample is plotted in Supplementary Figure 2. The temperature range from 4 K to 60 K is of most interest for optimally doped sample due to the low superconducting transition temperature

$T_C \sim 23$ K and no expected phase transitions above. We measure negligible change in the signal from superconductivity, as expected for the moderately high pump fluence used here.

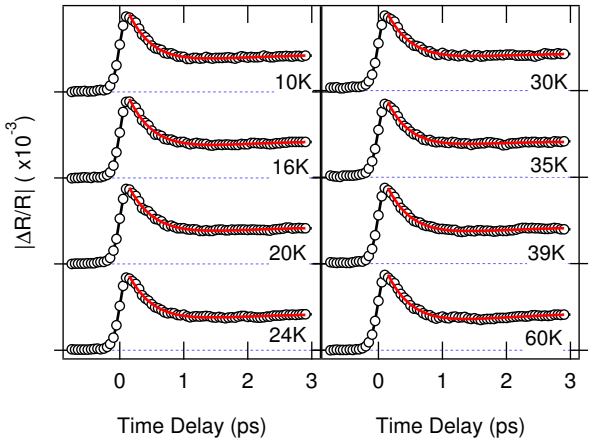

Figure 10: Differential reflectivity (black line, black circle) plotted together with bi-exponential fit function (red line) as function of temperature for the optimal doped sample, x = 0.074.

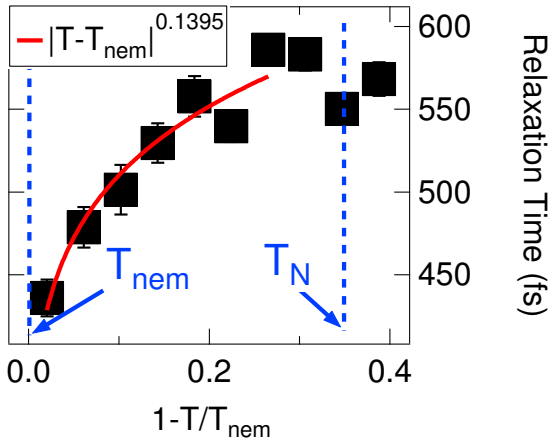

Figure 11: Underdoped sample: Critical behavior of the τ_{Fast} relaxation time approaching the nematic transition temperature.

Next we present differential reflectivity traces for the underdoped sample at select temperatures to illustrate the quality of fitting and data in Fig. 2(a). Here, each temperature is vertically offset for clarity.

As discussed in the main text, a critical speeding-up of the τ_{Fast} relaxation time is observed at temperatures slightly above the structural transition in the underdoped sample only. In Figure 10, we show the critical relaxation dynamics near T_S along with the corresponding fit. The fitting function is given by $\tau \propto \left|\frac{T}{T_C} - 1\right|^{-\nu z}$, where ν

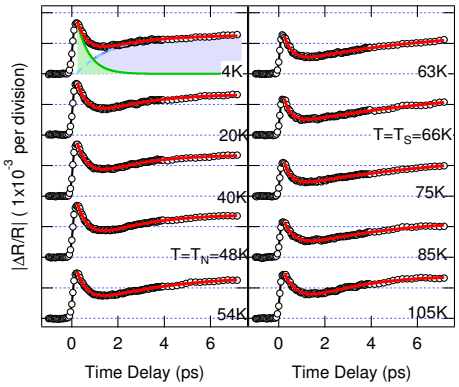

Figure 12: Raw temperature dependent traces (black) with fitting (red) for underdoped sample.

and z are the critical exponents representing the correlation length and the dynamical critical exponent respectively. We note that the time resolution of our setup limits measurements down $\sim 50fs$, yet the measured relaxation time at minimum is much larger, $\tau_{fast} \sim 400fs$). It is possible that the exact transition temperature lies within a range of +/- 2 K around 72 K. We find that letting $T_C = 73.5K$ gives the minimum error and results in $\nu z = 0.1395$.

[1] Y. Kamihara, T. Watanabe, M. Hirano, and H. Hosono, J. Am. Chem. Soc. **130**, 3296 (2008).

[2] P. C. Canfield, and S. L. Bud'ko, Annu. Rev. Cond. Mat. Phys. **1**, 27 (2010) and references therein.

[3] R. M. Fernandes, A. V. Chubukov, J. Knolle, I. Eremin, and J. Schmalian, Phys. Rev. B **85**, 024534 (2012).

[4] A. Patz, T. Li, S. Ran, R. M. Fernandes, J. Schmalian, S. L. Bud'ko, P. C. Canfield, I. E. Perakis, and J. Wang, Nat. Commun. **5**, 3229 (2014).

[5] R. M. Fernandes, A. V. Chubukov, and J. Schmalian, Nat. Phys. **10**, 97 (2014).

[6] M. Nakajima, *et. al.*, Proc. Natl. Acad. Sci. USA **108**, 12238 (2011).

[7] M. A. Tanatar, A. Kreyssig, S. Nandi, N. Ni, S. L. Bud'ko, P. C. Canfield, A. I. Goldman, and R. Prozorov, Phys. Rev. B **79**, 180508(R) (2009).

[8] J. Chu, J. G. Analytis, K. D. Greve, P. L. McMahon, Z. Islam, Y. Yamanoto, and I. R. Fisher, Science **329**, 824 (2010).

[9] S. Kasahara, *et. al.*, Nature **486**, 382 (2012).

[10] T. Li, A. Patz, L. Mouchliadis, J. Yan, T. A. Lograsso, I. E. Perakis, and J. Wang, Nature **496**, 69 (2013).

[11] Elbert E.M.. Chia, D. Talbayev, Jian-Xin. Zhu, H.Q. Yuan, T. Park, J.D. Thompson, C. Panagopoulos, G.F. Chen, J.F. Luo, N.L. Wang, and A.J. Taylor, Phys. Rev. Lett. **104**, 027003 (2010).

[12] A. Patz, T. Li, X. Liu, J. K. Furdyna, I. E. Perakis, and J. Wang, Phys. Rev. B **91**, 155108 (2015).

[13] J. Wang, G. A. Khodaparast, J. Kono, T. Slupinski, A. Oiwa, and H. Munekata, J. Supercond. **16**, 373 (2003).

[14] L. Rettig, R. Cortes, S. Thirupathaiah, P. Gegenwart, H. S. Jeevan, M. Wolf, J. Fink, and U. Bovensiepen, Phys. Rev. Lett. **108**, 097002 (2012).

[15] D. H. Torchinsky, G. F. Chen, J. L. Luo, N. L. Wang, and N. Gedik, Phys. Rev. Lett. **105**, 027005 (2010).

[16] J. Wang, G. A. Khodaparast, J. Kono, A. Oiwa, and H. Munekata, J. of Mod. Opt. **51(16-18)**, 2771 (2004); L. Luo, I. Chatzakis, A. Patz, and J. Wang, Phys. Rev. Lett. **114**, 107402 (2015); I. Chatzakis, L. Luo, J. Wang, N.-H. Shen, T. Koschny, J. Zhou, and C. M. Soukoulis, Phys. Rev. B **86**, 125110 (2012).

[17] K. W. Kim, A. Pashkin, H. Schafer, M. Beyer, M. Porer, T. Wolf, C. Bernhard, J. Demsar, R. Huber, and A. Leitenstorfer, Nat. Mater. **11**, 497 (2012).

[18] N. Ni, M. E. Tillman, J.-Q. Yan, A. Kracher, S. T. Hannahs, S. L. Bud'ko, and P. C. Canfield, Phys. Rev. B **78**, 214515 (2008).

[19] S. Nandi, *et. al.*, Phys. Rev. Lett. **104**, 057006 (2010).

[20] J. Wang, M. W. Graham, Y. Ma, G. R. Fleming, and R. A. Kaindl Phys. Rev. Lett. **104**, 177401 (2010); T. Li, L. Luo, M. Hupalo, J. Zhang, M. C. Tringides, J. Schmalian, and J. Wang, Phys. Rev. Lett. **108**, 167401 (2012);

[21] C. P. Grams, M. Valldor, M. Garst, and J. Hemberger, Nat. Commun. **5**, 4853 (2014).

[22] T. Shigenari, K. Abe, K. Morita, Qi Ping, E. Kojima, and H. Ino, J. Phys,: Condens. Matter **6**, 7469 (1994).

[23] Hacene Boukari, Matthew E. Briggs, J.N. Shaumeyer, and Robert W. Gammon, Phys. Rev. Lett. **65**, 21 (1990).

[24] A. Lucarelli, A. Dusza, F. Pfuner, P. Lerch, J. G. Analytis, J.-H. Chu, I. R. Fisher, and L. Degiorgi, New J. Phys. **12**, 073036 (2010).

[25] Temperatures for Γ_N are shifted by T=12K to match our transition temperatures as close as possible, since Lucarelli et al., measured a 5.1% doped sample with transition temperatures approximately 12K cooler than the 4.7% sample. We note the resisitivity data shows the same trend as ΔR/R and the U-shaped features match up very well with a 12K shift.

[26] S. Nandi, *et. al.,* Phys. Rev. Lett. **104**, 057006 (2010).

[27] F. L. Ning, K. Ahilan, T. Imai, A. S. Sefat, M. A. McGuire, B. C. Sales, D. Mandrus, P. Cheng, B. Shen, and H.-H. Wen, Phys. Rev. Lett. **104**, 037001 (2010).

[28] Q. Zhang, *et. al.,* Phys. Rev. Lett. **114**, 057001 (2015).

[29] D. K. Pratt, W. Tian, A. Kreyssig, J. L. Zarestky, S. Nandi, N. Ni, S. L. Bud'ko, P. C. Canfield, A. I. Goldman, and R. J. McQueeney, Phys. Rev. Lett. **103**, 087001 (2009).

[30] A. Dusza, A. Lucarelli, A. Sanna, S. Massidda, J.-H. Chu, I. R. Fisher, and L. Degiorgi, New J. Phys. **14**, 023020 (2012).

[31] H. J. Zeiger, J. Vidal, T. K. Cheng, E. P. Ippen, G. Dresselhaus, and M. S. Dresselhaus, Phys. Rev. B. **45**, 768 (1992).

[32] S. Kumar, L. Harnagea, S. Wurmehl, B. Buchner, and A. K. Sood, J. Phys. Soc. Jpn. **82**, 044715 (2013).

[33] Avigo, I., *et.al.*, Journ. Phys. Cond. Matt. **25**, 094003 (2013).